Hindawi Publishing Corporation
Mathematical Problems in Engineering
Volume 2014, Article ID 956895, 15 pages
http://dx.doi.org/10.1155/2014/956895

Research Article

Localization Accuracy of Range-Only Sensors with Additive and Multiplicative Noise

Xiufang Shi, Rong Zhang, and Zaiyue Yang

State Key Laboratory of Industrial Control Technology, Institute of Industrial Control Zhejiang University, Hangzhou, China

Correspondence should be addressed to Zaiyue Yang; yangzy@zju.edu.cn

Received 11 December 2013; Accepted 24 January 2014; Published 25 March 2014

Academic Editor: Zhengguang Wu

Copyright © 2014 Xiufang Shi et al. This is an open access article distributed under the Creative Commons Attribution License, which permits unrestricted use, distribution, and reproduction in any medium, provided the original work is properly cited.

The localization accuracy of range-only sensors with both additive and multiplicative noises is investigated. The main contributions consist of three parts. First, the Cramer-Rao Lower Bound (CRLB) of range-only localization system is derived, based on which the area of the uncertain ellipse about estimation is proposed as the metric to evaluate the localization accuracy. In addition, the analytical relationships between target-sensor distance and localization accuracy and between noise and localization accuracy are derived. Second, the metric is utilized to evaluate the localization accuracy for three important regular patterns of sensor deployment, that is, triangle, square, and hexagon. Two aspects of localization accuracy have been examined and discussed, respectively, for three patterns by numerical methods, including (a) the geometric distribution of localization accuracy and (b) the average localization accuracy. Both theoretical and numerical results show that the multiplicative noise will influence significantly the localization accuracy. Third, on a lab-scale ultrasonic range-only sensor system the existence of additive and multiplicative noises is verified. It is also shown that the experimental localization accuracy is close to the previously analyzed theoretical accuracy.

1. Introduction

It is well known that target localization plays an important role in military and security [1], which is also the foundation of other advanced tasks, for example, target tracking. With the great development of electronics in recent years, wireless sensor networks (WSN) based target localization systems have attracted increasing research interests [1–9]. Several kinds of sensors are widely used to collect the necessary information, for example, range-only sensors [2, 10], angle of arrival (AOA) sensors [10–12], time of arrival (TOA) sensors [10], and time difference of arrival (TDOA) sensors [10]. In a WSN based localization system, the target localization problem is essentially an estimation problem. That is, a number of sensors are deployed to collect the position-related data of the target; then the data are sent to the leader node to estimate the position of the target.

In the context of statistical signal processing, the Cramer-Rao Lower Bound (CRLB) is regarded as the most important benchmark to assess the estimation accuracy of an unbiased estimator [13–16]. Therefore, CRLB is widely used in the localization system to evaluate the localization accuracy [1, 17–21]. It is also of great significance in sensor selection and deployment, motion coordination, and dynamic sensor collaboration [7, 11, 22]. With regard to different measurement models, CRLB can be derived in various forms. For example, CRLB of the widely used range-only localization system is a matrix of target-sensor azimuth angle in previous literature [10].

However, it is notable that this result is derived under the assumption that the measurements consist of only additive noise [10]. In other words, this assumption ignores the multiplicative noise that indeed reflects the effect of target-sensor distance on measurement error. However, [2] argues that in a lot of occasions multiplicative noise cannot be neglected, and the measurement error will increase significantly with the increase of target-sensor distance. In fact, the experimental results in [2] even show that multiplicative noise is 3 to 4 times larger than additive noise. Unfortunately, very few studies take multiplicative noise into consideration when deriving CRLB and assessing localization accuracy for the range-only localization system.

In this paper, the localization accuracy problem of range-only sensors with both additive and multiplicative noises is investigated. The main contributions can be summarised as below.

(1) Theoretically, CRLB of range-only localization system is deduced based on a more general measurement model with both additive and multiplicative noise. Then, a metric is proposed based on CRLB to evaluate the localization accuracy, and three important properties of this metric are derived. The properties indicate, surprisingly, that shorter target-sensor distance does not always lead to better localization accuracy, and proper distance will yield the best accuracy under a certain situation.

(2) Numerically, the localization accuracy for three regular patterns of sensor deployment, that is, triangle, square, and hexagon, has been evaluated by the proposed metric. For each pattern, two aspects of localization accuracy have been examined and discussed, including (a) geometric distribution of localization accuracy and (b) average localization accuracy. To the best of our knowledge, there is no such extensive analysis about the localization accuracy for regular deployment patterns. Numerical results show that the multiplicative noise will influence significantly the localization accuracy and also provide some important guidelines for optimal sensor deployment.

(3) Experimentally, the existence of multiplicative noise on a lab-scale ultrasonic range-only sensor system is verified and the corresponding parameters are computed. Then, the experimental localization accuracy is calculated based on real data, which is very close to the theoretical accuracy.

The rest of this paper is organized as follows. In Section 2, the measurement model of range-only localization system with both additive and multiplicative noise is introduced. Then, CRLB, the metric, and its properties are derived in Section 3. Section 4 presents the numerical analysis and discussion about the localization accuracy in terms of the proposed metric in regular deployment patterns. The experiment is presented in Section 5 and the conclusion is drawn in Section 6.

2. Measurement Model

Without loss of generality, we will consider the localization problem for a single stationary target in two-dimensional field in this paper. The presented results can be readily extended to three-dimensional cases and are also the foundation of target tracking tasks.

Let the localization system consist of N homogeneous range-only sensors, whose positions are known a priori. Let the coordinate of the ith sensor be (x_i, y_i), and let the coordinate of the target be (x, y). Then, the true distance between the target and sensor i can be expressed as

$$r_i = \sqrt{(x_i - x)^2 + (y_i - y)^2}. \tag{1}$$

Being different from most previous studies [10], which adopt the sensor measurement with only additive noise, a more general model with both additive and multiplicative noise [2] is considered here:

$$z_i = (1 + \omega_i) r_i + v_i, \tag{2}$$

where z_i denotes the measurement of the ith sensor and ω_i and v_i are, respectively, multiplicative noise and additive noise in the ith sensor.

Assume that ω_i and v_i are independent white Gaussian noises, that is, $\omega_i \sim N(\mu_\omega, \sigma_\omega^2)$, $v_i \sim N(\mu_v, \sigma_v^2)$, which are also independent of those in the other sensors. From (2), the total measurement noise of sensor i is $n_i = r_i\omega_i + v_i$. Clearly, it is still white Gaussian noise with the following mean and variance:

$$\mu_i = r_i\mu_\omega + \mu_v, \tag{3}$$

$$\sigma_i^2 = r_i^2\sigma_\omega^2 + \sigma_v^2. \tag{4}$$

Therefore, the measurement z_i also follows normal distribution:

$$z_i \sim N\left(\mu_i + r_i, \sigma_i^2\right). \tag{5}$$

Then, consider the entire localization system that consists of N sensors. Similar to (5), the measurement vector of N sensors follows an N-dimensional normal distribution:

$$Z(\theta) \sim N\left(\mu(\theta), C(\theta)\right), \tag{6}$$

where $\theta = [x, y]^T$, $Z(\theta) = [z_1, z_2, \ldots, z_N]^T$, $\mu(\theta) = [\mu_1 + r_1, \mu_2 + r_2, \ldots, \mu_N + r_N]^T$, and $C(\theta) = \mathrm{diag}\{\sigma_1^2, \sigma_2^2, \ldots, \sigma_N^2\}$.

Remark 1. From (3) and (4), it can be found that both the mean μ_i and the variance σ_i^2 associated with sensor i are closely related to target-sensor distance r_i. In particular, the variance σ_i^2 will grow in a rapid speed with the increase of r_i.

For a target at (x, y), the probability density function (PDF) of measurement of sensor i can be readily obtained according to (5):

$$p(z_i \mid \theta) = \frac{1}{\sqrt{2\pi\sigma_i^2}} \exp\left[-\frac{(z_i - r_i - \mu_i)^2}{2\sigma_i^2}\right]. \tag{7}$$

Since the measurements of different sensors are independent, the joint PDF of the entire localization system with N sensors can be written as

$$p(Z \mid \theta) = \prod_{i=1}^{N} p(z_i \mid x, y). \tag{8}$$

3. CRLB and Metric

In this section, CRLB of range-only localization system with both additive and multiplicative noise is derived and a metric is proposed to evaluate the localization accuracy. Then, three important analytical properties about the relationships between target-sensor distance and localization accuracy and between noise and localization accuracy are derived.

3.1. Derivation of CRLB. It is well known that CRLB is the lower bound for the variance of any unbiased estimate. Thus, it is widely utilized in practice as an important benchmark to evaluate the estimation accuracy of an estimator [13–16, 23, 24]. The inverse of CRLB is the so-called Fisher Information Matrix (FIM), which stands for the amount of information contained in data.

By referring the definition of FIM in [13], an entry of FIM denoted as F_{lk} is

$$F_{lk} = -E\left[\frac{\partial^2 \ln p(Z \mid \theta)}{\partial\theta_l \partial\theta_k}\right], \tag{9}$$

where $l, k = 1, 2$, $\theta_1 = x$, and $\theta_2 = y$. Therefore, the corresponding FIM can be expressed as

$$\begin{aligned} F &= \begin{bmatrix} F_{11} & F_{12} \\ F_{21} & F_{22} \end{bmatrix} \\ &= -E\begin{bmatrix} \dfrac{\partial^2 \ln(p(Z \mid x, y))}{\partial x^2} & \dfrac{\partial^2 \ln(p(Z \mid x, y))}{\partial x \partial y} \\ \dfrac{\partial^2 \ln(p(Z \mid x, y))}{\partial x \partial y} & \dfrac{\partial^2 \ln(p(Z \mid x, y))}{\partial y^2} \end{bmatrix}. \end{aligned} \tag{10}$$

Alternatively, since the measurement given in (6) is Gaussian with nonzero mean, the entry of FIM can also be computed as below [13]:

$$\begin{aligned} F_{lk} = &\left[\frac{\partial\mu(\theta)}{\partial\theta_l}\right]^T C^{-1}(\theta)\left[\frac{\partial\mu(\theta)}{\partial\theta_k}\right] \\ &+ \frac{1}{2} tr\left[C^{-1}(\theta)\frac{\partial C(\theta)}{\partial\theta_l} C^{-1}(\theta)\frac{\partial C(\theta)}{\partial\theta_k}\right]. \end{aligned} \tag{11}$$

Because the measurements of different sensors are independent, the complete FIM of the entire localization system is the sum of the individual FIM associated with each sensor [13]. Then, taking (1), (3), and (4) into (11), we have

$$\begin{aligned} F_{11} &= \sum_{i=1}^{N} \frac{1}{\sigma_i^4}\left\{\sigma_i^2\left[(1+\mu_\omega)\frac{x_i - x}{r_i}\right]^2 + \frac{1}{2}\left[2\sigma_\omega^2(x_i - x)\right]^2\right\}, \\ F_{12} = F_{21} &= \sum_{i=1}^{N} \frac{1}{\sigma_i^4}\left[\sigma_i^2(1+\mu_\omega)^2\frac{(x_i - x)}{r_i}\frac{(y_i - y)}{r_i}\right. \\ &\qquad \left. + 2\sigma_\omega^4(x_i - x)(y_i - y)\right], \\ F_{22} &= \sum_{i=1}^{N} \frac{1}{\sigma_i^4}\left\{\sigma_i^2\left[(1+\mu_\omega)\frac{y_i - y}{r_i}\right]^2 + \frac{1}{2}\left[2\sigma_\omega^2(y_i - y)\right]^2\right\}. \end{aligned} \tag{12}$$

Let φ_i denote the azimuth angle of sensor i relative to the target. Obviously, we have $\cos\varphi_i = (x_i - x)/r_i$, $\sin\varphi_i = (y_i - y)/r_i$. As a result, the complete FIM of N sensors can be rewritten into the following compact form:

$$F = \sum_{i=1}^{N} g_i \begin{bmatrix} \cos^2\varphi_i & \cos\varphi_i \sin\varphi_i \\ \cos\varphi_i \sin\varphi_i & \sin^2\varphi_i \end{bmatrix}, \tag{13}$$

where g_i is a function of noise and target-sensor distance of sensor i :

$$g_i = \frac{1}{\sigma_i^4}\left[\sigma_i^2(1+\mu_\omega)^2 + 2\sigma_\omega^4 r_i^2\right]. \tag{14}$$

At last, the corresponding CRLB can be expressed as

$$\text{CRLB} = F^{-1}. \tag{15}$$

Remark 2. Similar to previous studies, for example, [1, 2, 12], in this paper we will assume that all estimates of the target position are unbiased. Therefore, the derived CRLB corresponds to the lower bound that the variance of position estimate can achieve. That is, it can be regarded as the representation of localization accuracy. However, since CRLB is a 2×2 matrix with very complex entries, it is difficult to use and to analyze in the evaluation of localization accuracy. Therefore, a scalar metric will be proposed in the next subsection, which can replace the complicated CRLB and approximately represent the localization accuracy.

3.2. A Novel Metric. Geometrically, CRLB defines an ellipse of estimation errors in both x-axis and y-axis [10]. Let λ_1 and λ_2 denote the eigenvalues of CRLB, and consequently $\sqrt{\lambda_1}$ and $\sqrt{\lambda_2}$ represent the length of x-axis and y-axis of the ellipse [10]. Then, the area of the ellipse is $\pi\sqrt{\lambda_1\lambda_2}$, which reflects the localization accuracy. That is, a smaller ellipse area indicates a more accurate estimation of target position. For simplicity, the constant π is dropped and let

$$\mathfrak{R} = \sqrt{\lambda_1\lambda_2} \tag{16}$$

be the metric of localization accuracy. Note that

$$\lambda_1\lambda_2 = \det\{\text{CRLB}\} = \frac{1}{\det\{F\}}, \tag{17}$$

$$\det\{F\} = \frac{1}{2}\sum_{i=1}^{N}\sum_{j=1}^{N} g_i g_j \sin^2(\varphi_{ij}), \tag{18}$$

where $\varphi_{ij} = \varphi_i - \varphi_j$ is the intersection angle between the line of sensor i to target and the line of sensor j to target. Consequently, taking (17) and (18) into (16) yields

$$\mathfrak{R} = \sqrt{\frac{1}{\det\{F\}}} = \sqrt{\frac{2}{\sum_{i=1}^{N}\sum_{j=1}^{N} g_i g_j \sin^2(\varphi_{ij})}}. \tag{19}$$

Remark 3. In some previous studies [10, 19], $\lambda_1\lambda_2$ is also used as a metric, which is the so-called D-Criterion. Since it is monotonic to $\mathfrak{R}$, it can reflect the variation trend of localization accuracy to some extent. However, it is important to notice that the D-Criterion is nonlinear to the area of ellipse of estimation error; thus, the scale to quantify the localization accuracy will be distorted. In assessing the average localized accuracy, it would be useful to have a scale which is linear to the area of ellipse. This is achieved by using $\mathfrak{R}$ as the metric.

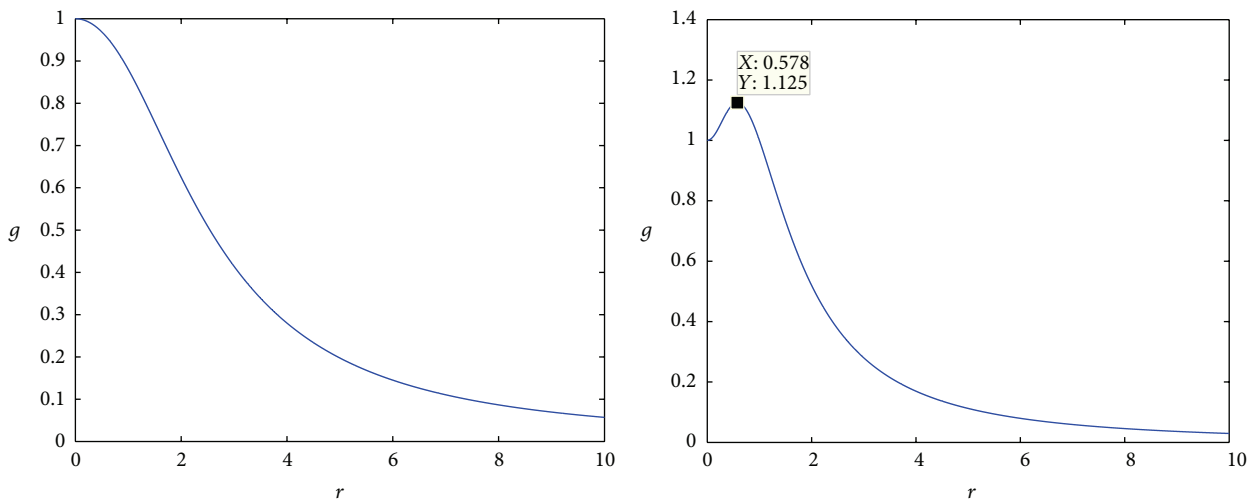

(a) $\sigma_\omega^2 = 0.25, \mu_\omega = 0$ (b) $\sigma_\omega^2 = 1, \mu_\omega = 0$

FIGURE 1: The profiles of g_i over r_i with different variance of multiplicative noise. Let additive noise be $\upsilon \sim N(0,1)$ and let multiplicative noise satisfy (a) $2\sigma_\omega^2 < (1+\mu_\omega)^2$; (b) $2\sigma_\omega^2 \geq (1+\mu_\omega)^2$. The x and y axes are r_i and g_i.

Remark 4. From [10], $\mathfrak{R}$ of additive noise measurement model is

$$\mathfrak{R} = \sqrt{\frac{2}{\sum_{i=1}^{N}\sum_{j=1}^{N}\left(1/\sigma_\upsilon^4\right)\sin^2\left(\varphi_{ij}\right)}}. \tag{20}$$

It is clear that (20) is a special case of (19). For a localization system with only additive noise, multiplicative noise does not exist; that is, $\sigma_\omega^2 = 0$, $\mu_\omega = 0$. Therefore, $g_i = 1/\sigma_\upsilon^2$ from (14) and $\mathfrak{R}$ retreats to a more simple form that only depends on the intersection angle φ_{ij}.

3.3. Analytical Properties of $\mathfrak{R}$. Analytical properties of $\mathfrak{R}$ will be derived in this part, which indeed reveal very interesting results about the relationships between $\mathfrak{R}$ and the target-sensor distance, and between $\mathfrak{R}$ and the noise. In the following paragraphs, we will first derive the relationship between $\mathfrak{R}$ and g_i and then the relationship between g_i and r_i and at last the relationship between g_i and σ_ω^2. The first property can be directly observed from (19).

Property 1. $\mathfrak{R}$ is a strictly monotonically decreasing function of g_i.

Property 2. The relationship between g_i and target-sensor distance r_i depends on the mean and variance of multiplicative noise as follows.

(i) If $2\sigma_\omega^2 < (1+\mu_\omega)^2$, g_i is a strictly monotonically decreasing function of r_i.

(ii) If $2\sigma_\omega^2 \geq (1+\mu_\omega)^2$, g_i is a strictly monotonically increasing function of r_i when $r_i^2 < T_r$, and g_i is a strictly monotonically decreasing function of r_i when $r_i^2 > T_r$. g_i achieves the maximum value $g_{\max} = (2\sigma_\omega^2+1)^2/8\sigma_\upsilon^2\sigma_\omega^2$ at $r_i^2 = T_r$, where

$$T_r = \frac{\sigma_\upsilon^2\left(2\sigma_\omega^2 - (1+\mu_\omega)^2\right)}{\sigma_\omega^2\left(2\sigma_\omega^2 + (1+\mu_\omega)^2\right)}. \tag{21}$$

Proof. The proof of Property 2 is straightforward. The partial derivative of g_i with respect to r_i can be written as follows:

$$\begin{aligned}\frac{\partial g_i}{\partial r_i} = &\left(\left\{-\sigma_\omega^2\left[2\sigma_\omega^2 + (1+\mu_\omega)^2\right]r_i^2\right.\right.\\ &\left.\left.+\sigma_\upsilon^2\left[2\sigma_\omega^2 - (1+\mu_\omega)^2\right]\right\}2\sigma_\omega^2 r_i\right)\\ &\times\left(\left(\sigma_\upsilon^2 + \sigma_\omega^2 r_i^2\right)^3\right)^{-1}.\end{aligned} \tag{22}$$

The denominator of $\partial g/\partial r_i$ is always positive. If $2\sigma_\omega^2 < (1+\mu_\omega)^2$, the numerator of $\partial g/\partial r_i$ is negative; then $\partial g/\partial r_i < 0$ and g_i is a strictly monotonically decreasing function of r_i. Otherwise, if $2\sigma_\omega^2 \geq (1+\mu_\omega)^2$, the monotonicity of g_i is related to r_i. When $r_i^2 < T_r$, $\partial g/\partial r_i > 0$, thus g_i is a strictly monotonically increasing function of r_i; when $r_i^2 > T_r$, $\partial g/\partial r_i < 0$, thus g_i is a strictly monotonically decreasing function of r_i. g_i achieves the maximum at T_r. The proof is completed. □

Figure 1 illustrates the profiles of g_i over r_i with different σ_ω^2. In accordance with the two aforementioned properties, the relationship between r_i and $\mathfrak{R}$ can be readily conducted.

Remark 5. Due to the existence of multiplicative noise, $\mathfrak{R}$ becomes more complicated and is affected by both target-sensor distance and intersection angle. For the localization system with only additive noise, it is widely accepted only

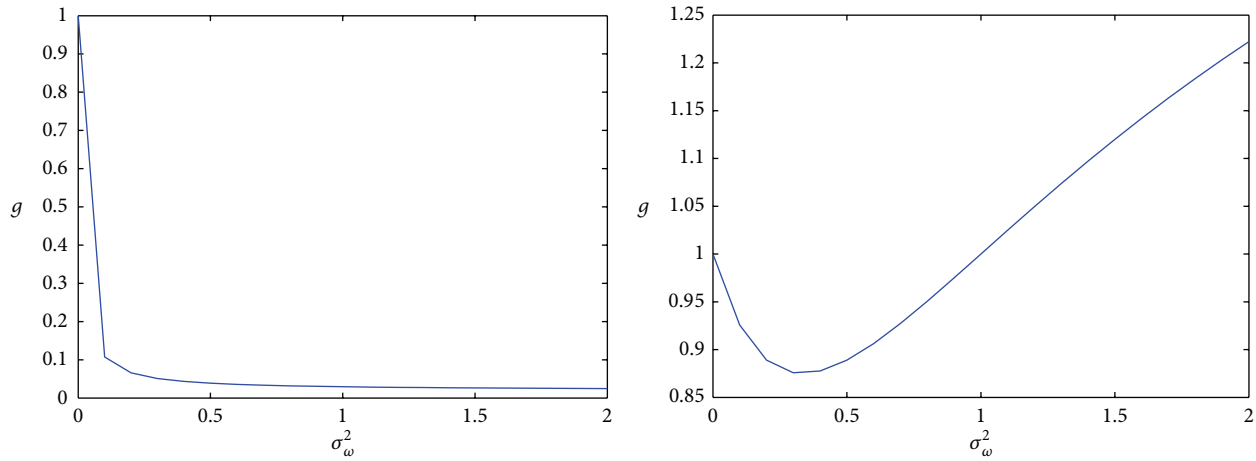

(a) $r_i = 10$ (b) $r_i = 1$

FIGURE 2: The profiles of g_i over σ_ω^2 with different target-sensor distance r_i. Let additive noise be $v \sim N(0, 1)$ and let the target-sensor distance r_i satisfy (a) $r_i^2 > 4\sigma_v^2/(1 + \mu_\omega)^2$; (b) $r_i^2 \leq 4\sigma_v^2/(1 + \mu_\omega)^2$. The x and y axes are σ_ω^2 and g_i.

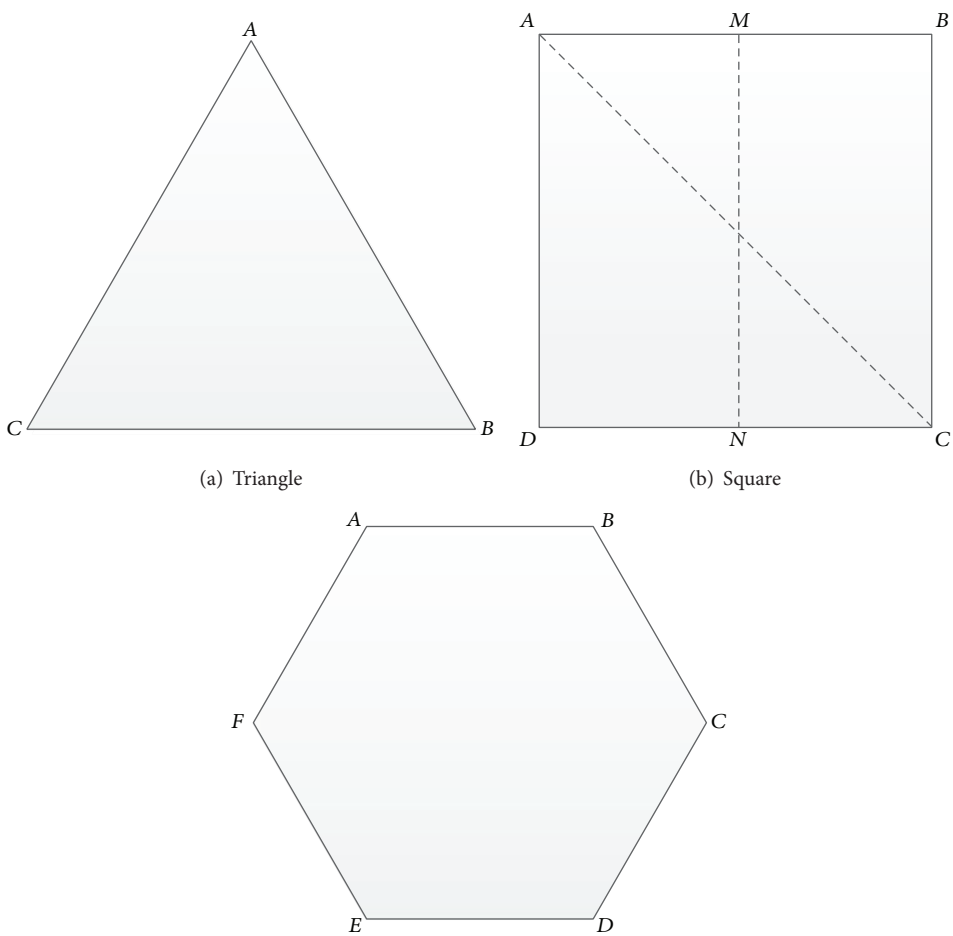

(a) Triangle (b) Square

(c) Hexagon

FIGURE 3: Three kinds of regular deployment patterns, each vertex means a sensor node.

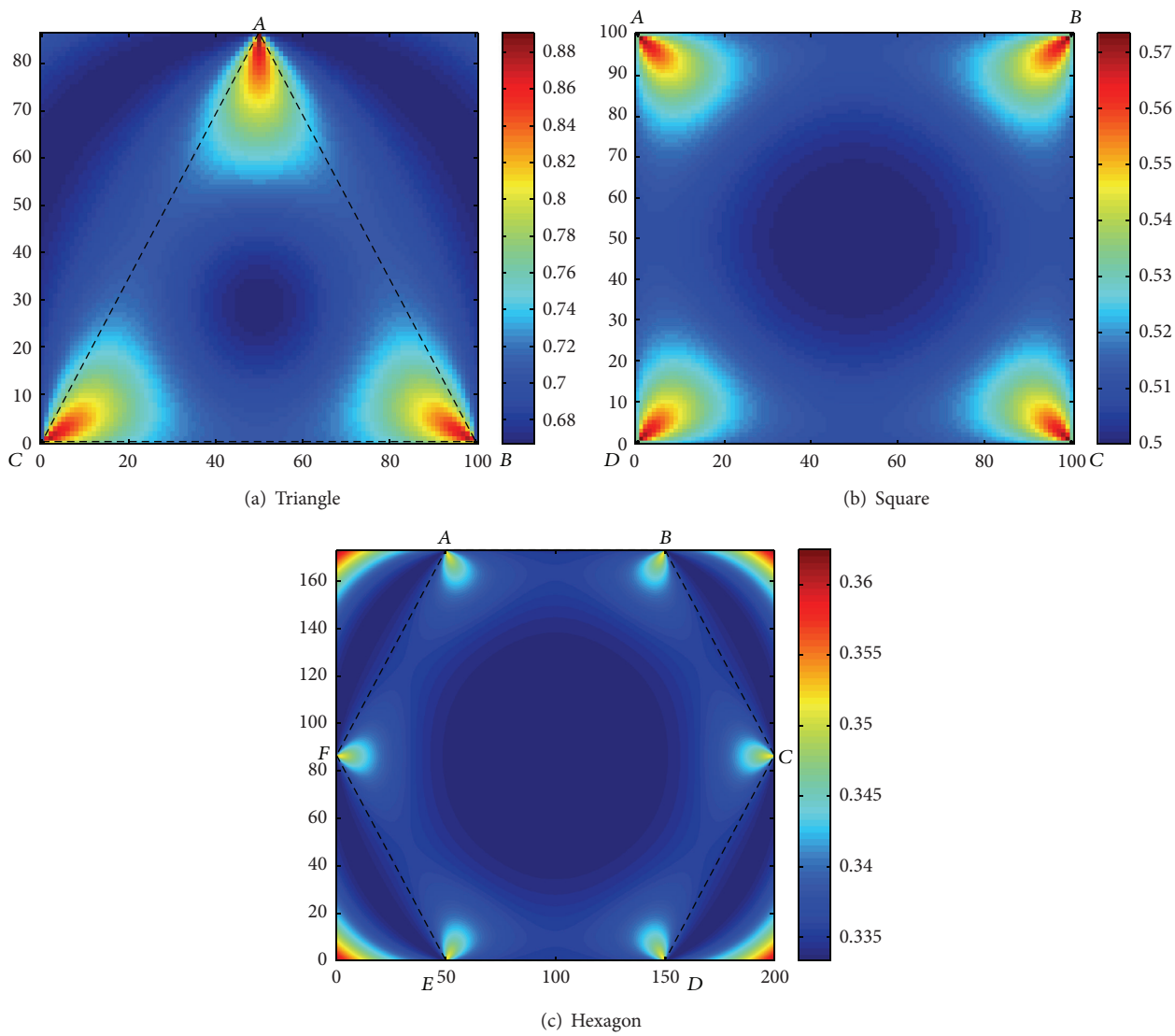

FIGURE 4: Distribution of $\mathfrak{R}$ under three kinds of regular patterns with $\sigma_\omega^2 = 0$ and $\sigma_\upsilon^2 = 1$.

that the good angular diversity can lead to a low $\mathfrak{R}$, namely, an accurate estimation of target position [10]. However, for the localization system with both additive and multiplicative noises according to Property 2, both a good angular diversity and a proper distance are necessary to yield the best localization accuracy. Surprisingly, a shorter distance does not necessarily lead to a better accuracy, and $r_i^2 = T_r$ will yield the best accuracy under a certain circumstance.

Property 3. (i) The relationship between g_i and additive noise: g_i is a strictly monotonically decreasing function of σ_υ^2.

(ii) The relationship between g_i and multiplicative noise:

(a) if $r_i^2 > 4\sigma_\upsilon^2/(1+\mu_\omega)^2$, g_i is a strictly monotonically decreasing function of σ_ω^2;

(b) if $r_i^2 \le 4\sigma_\upsilon^2/(1+\mu_\omega)^2$, g_i is a strictly monotonically increasing function of σ_ω^2 when $\sigma_\omega^2 > T_{\sigma_\omega^2}$, and g_i is a strictly monotonically decreasing function of σ_ω^2 when $\sigma_\omega^2 \le T_{\sigma_\omega^2}$, where

$$T_{\sigma_\omega^2} = \frac{(1+\mu_\omega)^2\sigma_\upsilon^2}{4\sigma_\upsilon^2 - (1+\mu_\omega)^2 r_i^2}. \tag{23}$$

Proof. The proof of Property 3 is straightforward.

(i) The partial derivative of g_i with respect to σ_υ^2 is

$$\frac{\partial g_i}{\partial \sigma_\upsilon^2} = -\frac{(1+\mu_\omega)^2}{\sigma_i^4} - \frac{4\sigma_\omega^4 r_i^2}{\sigma_i^6} < 0. \tag{24}$$

Then g_i is a strictly monotonically decreasing function of σ_υ^2.

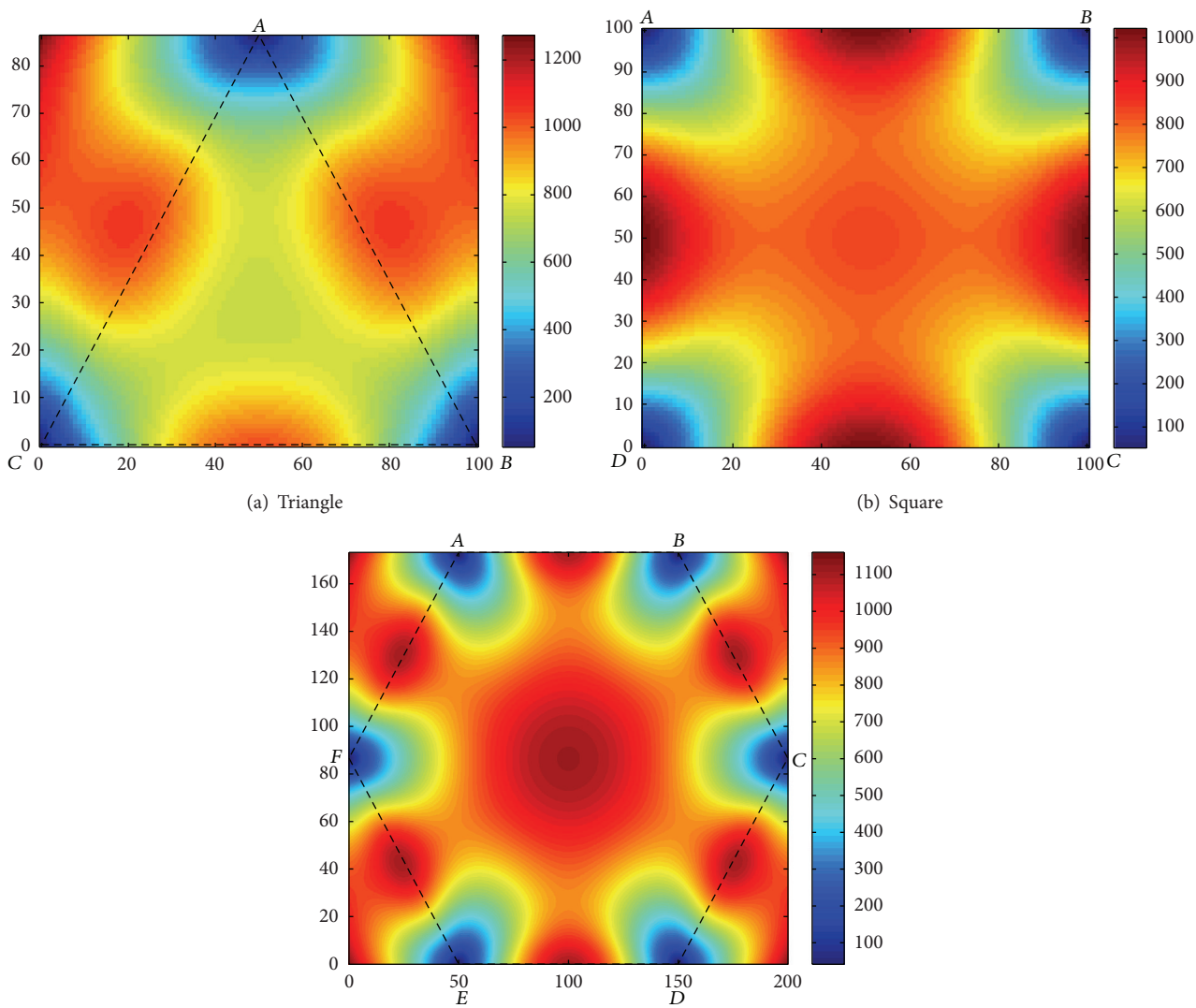

(a) Triangle

(b) Square

(c) Hexagon

Figure 5: Distribution of $\mathfrak{R}$ under three kinds of regular patterns with $\sigma_\omega^2 = 1$ and $\sigma_v^2 = 1$.

(ii) The partial derivative of g_i with respect to σ_ω^2 can be written as follows:

$$\frac{\partial g_i}{\partial \sigma_\omega^2} = \frac{r_i^2}{\sigma_i^6}\left[\sigma_\omega^2\left(4\sigma_v^2 - (1+\mu_\omega)^2 r_i^2\right) - (1+\mu_\omega)^2\sigma_v^2\right]. \tag{25}$$

In (25), r_i^2/σ_i^6 is always positive. If $r_i^2 > 4\sigma_v^2/(1+\mu_\omega)^2$, $\sigma_\omega^2(4\sigma_v^2 - (1+\mu_\omega)^2 r_i^2)$ is negative; then $\partial g_i/\partial\sigma_\omega^2 < 0$ and g_i is a strictly monotonically decreasing function of σ_ω^2. Otherwise, if $r_i^2 \le 4\sigma_v^2/(1+\mu_\omega)^2$, the monotonicity of g_i is related to σ_ω^2. When $\sigma_\omega^2 > T_{\sigma_\omega^2}$, $\partial g_i/\partial\sigma_\omega^2 > 0$, thus g_i is a strictly monotonically increasing function of σ_ω^2; when $\sigma_\omega^2 \le T_{\sigma_\omega^2}$, $\partial g_i/\partial\sigma_\omega^2 \le 0$, thus g_i is a strictly monotonically decreasing function of σ_ω^2.

The proof is completed. □

Figure 2 illustrates the profiles of g_i over σ_ω^2 with different target-sensor distance r_i. In accordance with Properties 1 and 3, the relationship between σ_ω^2 and $\mathfrak{R}$ can be readily conducted.

Remark 6. From Property 3(ii), surprisingly, we can conclude that the increase of multiplicative noise may not necessarily reduce the localization accuracy. When $r_i^2 \le 4\sigma_v^2/(1+\mu_\omega)^2$, with the further increase of σ_ω^2, g_i will also increase and the accuracy will be improved. However, two points should be noticed. First, $\lim_{\sigma_\omega^2\to\infty} g_i = 2/r_i^2$; therefore, g_i is upper

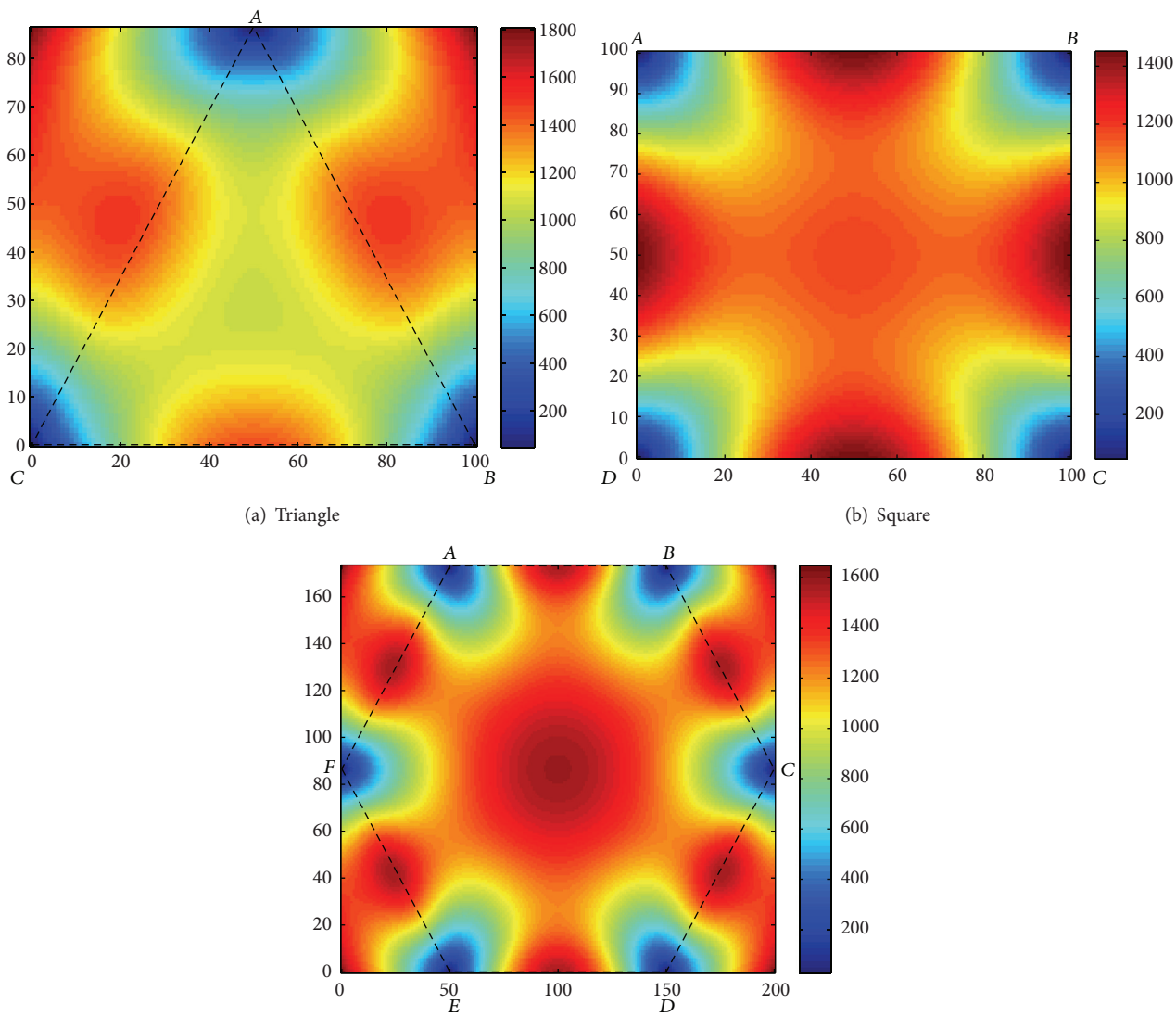

(a) Triangle

(b) Square

(c) Hexagon

FIGURE 6: Distribution of $\mathfrak{R}$ under three kinds of regular patterns with $\sigma_\omega^2 = 3$ and $\sigma_v^2 = 1$.

bounded by the constant $2/r_i^2$ even if σ_ω^2 is infinite. Second, in practice the target-sensor distance r_i is much larger than σ_v^2; therefore, $r_i^2 > 4\sigma_v^2/(1+\mu_\omega)^2$ always holds and case (b) barely exists in applications.

4. Numerical Analysis of $\mathfrak{R}$ under Different Sensor Deployment Patterns

In practice, it is usually desirable for target localization systems to deploy sensors in regular patterns. The regular deployment patterns outperform other irregular ones in many aspects, such as the convenience of deployment, a high degree of coverage, and connectivity [25]. Nevertheless, the localization accuracy under different regular patterns is rarely discussed. To this end, the localization accuracy of range-only localization system with both additive and multiplicative noises will be studied in this section. Three most important regular patterns will be investigated, that is, triangle, square, and hexagon, which indeed are the basic elements to form a large localization system. From (13), (18), and (19), it is clear that $\mathfrak{R}$ is a complicated function of noise, intersection angle φ_{ij}, and target-sensor distance r_i. In addition, for a given deployment pattern the sensors are fixed; thus, both φ_{ij} and r_i are complicated functions of the target position (x, y). That is, $\mathfrak{R}$ becomes an extremely complicated function of noise and (x, y). As a result, theoretical analysis of $\mathfrak{R}$ with respect to the variations of noise and (x, y) seems impossible. Therefore, numerical study will be conducted in this section. Due to page limitation, the numerical experiments will be carried out only for several typical parameter settings, which, however, are able to reveal the primary properties of $\mathfrak{R}$.

4.1. Distribution of $\mathfrak{R}$. In this subsection, the distribution of $\mathfrak{R}$ inside the three regular patterns, that is, triangle, square,

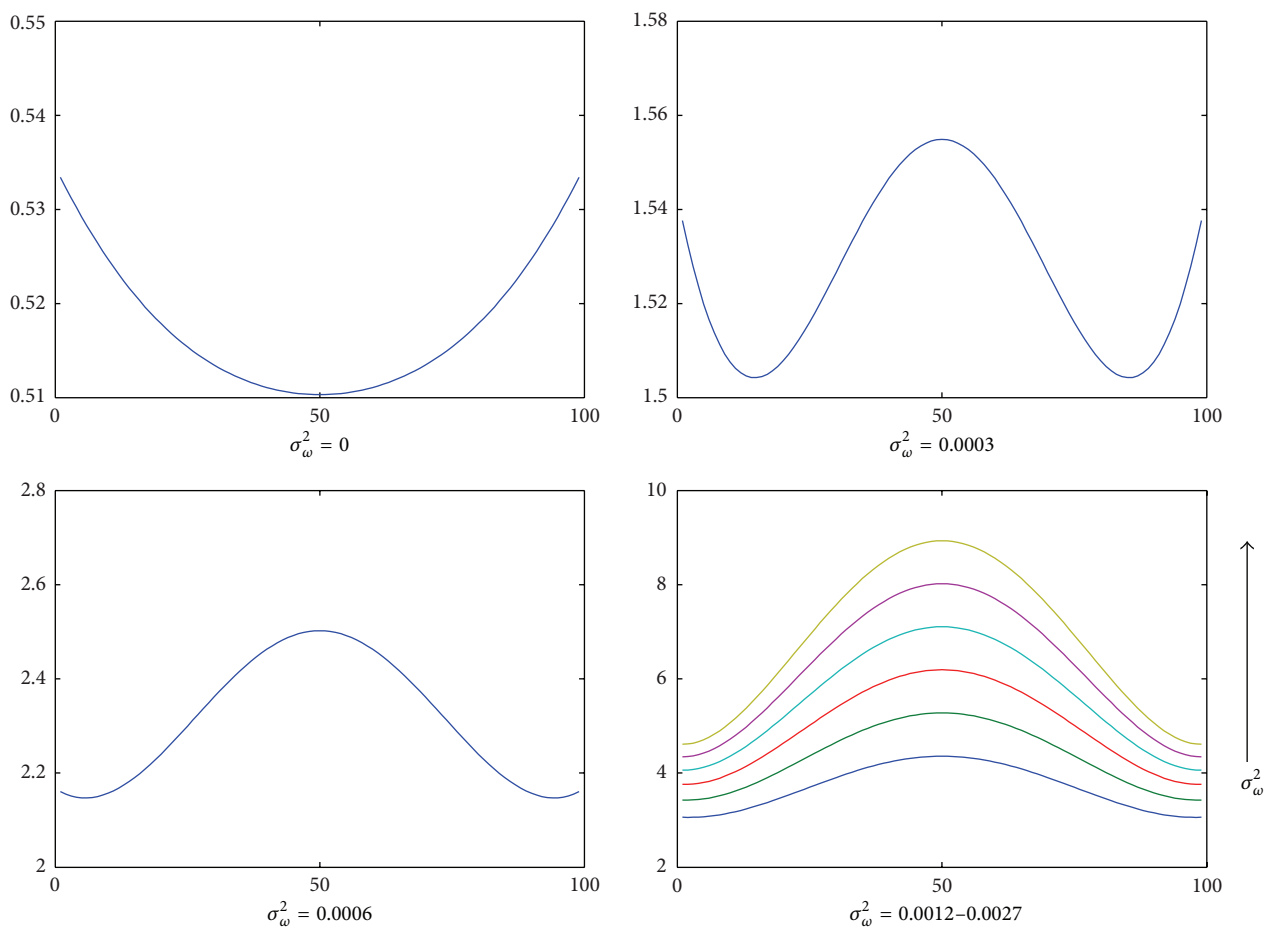

Figure 7: The profiles of $\mathfrak{R}$ under the effect of multiplicative noise with target moving along AB. The x-axis and y-axis are the distance between target and sensor A and $\mathfrak{R}$.

and hexagon, will be investigated. Since the effect of additive noise on $\mathfrak{R}$ is relatively simple, we will mainly focus on the impact of multiplicative noise. To this end, let the variance of additive noise be constant for simplicity, that is, $\sigma_\upsilon^2 = 1$, and assume that both additive and multiplicative noises are zero-mean white Gaussian noise; that is, $\mu_\omega = \mu_\upsilon = 0$. The work in [2] indicates that in practice the distance between sensors is much larger than noise disturbance; therefore, let the side length of regular patterns be $a = 100$. As the experimental results in [2] also suggest that multiplicative noise is 3 to 4 times larger than additive noise, let the variance of multiplicative noise be $\sigma_\omega^2 = 0, 1, 3$, and the corresponding distributions of $\mathfrak{R}$ are shown in Figures 4, 5, and 6, respectively.

In Figure 4 with only additive noise, it is clear that the lowest $\mathfrak{R}$ always locates at the inner center of the three regular patterns. That is, the inner center achieves the best localization accuracy. On the other hand, the worst localization accuracy is located near the sensors for all patterns. This is because under additive noise, the target-sensor distance is irrelevant to localization accuracy, and the point with the best angular diversity, that is, the inner center, yields the best accuracy.

Figures 5 and 6 show that the distribution of $\mathfrak{R}$ under both additive and multiplicative noises is completely different from that under additive noise. For all patterns, the points with the best localization accuracy are located at the active sensors, while the points with poor accuracy are located at the inner centers and the midpoints on each side. It is clear that, due to the existence of multiplicative noise, the target-sensor distance significantly influences the distribution of $\mathfrak{R}$. For more details, the profiles of $\mathfrak{R}$ along some representative lines will be examined next.

Without loss of generality, the square will be studied and similar results can readily be obtained for triangle and hexagon. Let us look at the side line AB, the diagonal line AC, and midline MN of the square in Figure 3(b), and the corresponding profiles of $\mathfrak{R}$ are shown in Figures 7, 8, and 9. It is clear that the minimal points of $\mathfrak{R}$ are driven from the central points to sides and corners with the increase of σ_ω^2. In addition, the shape of profile will be maintained when σ_ω^2 is larger than a very small value, which also suggests that

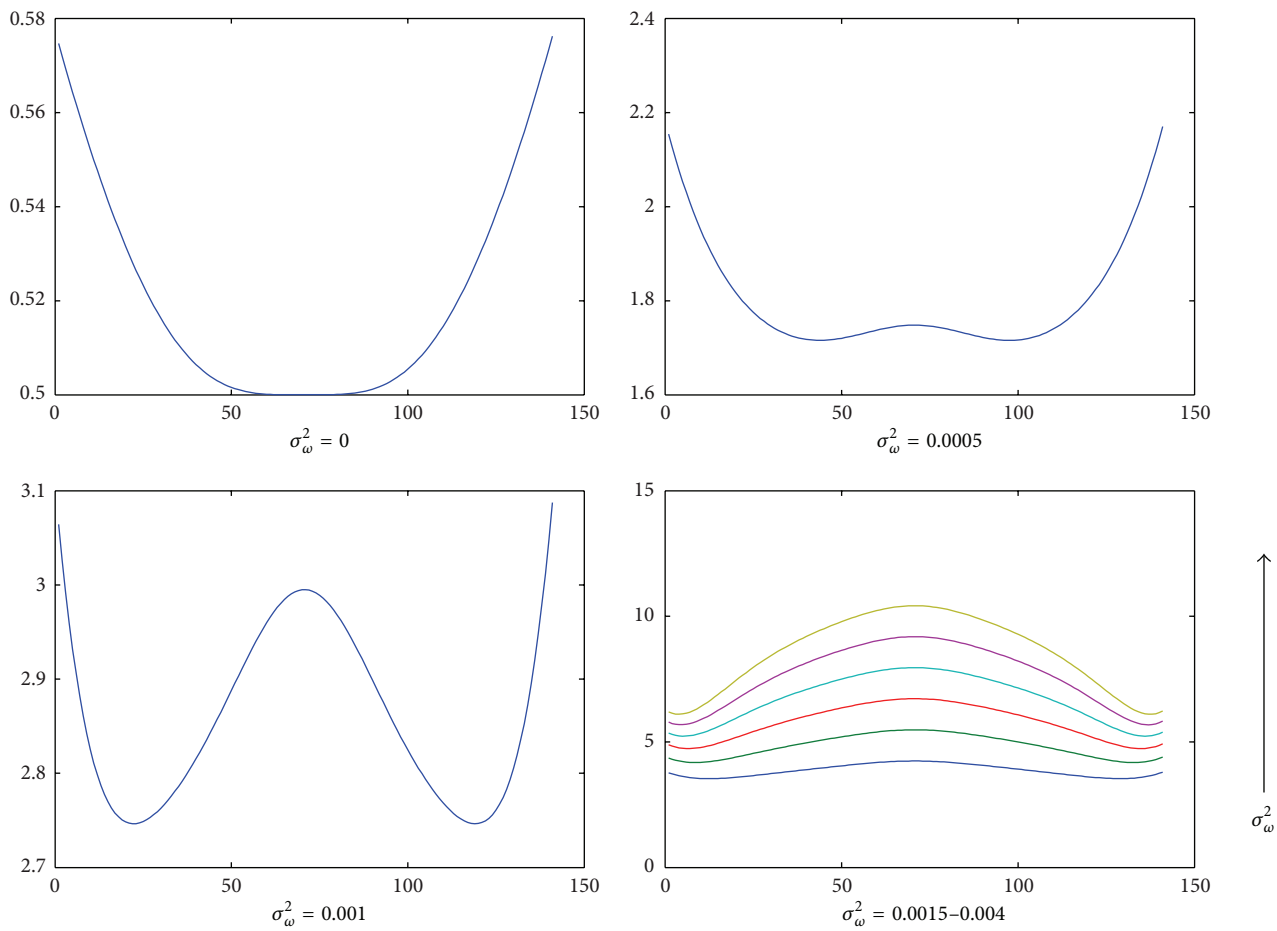

Figure 8: The profiles of $\mathfrak{R}$ under the effect of multiplicative noise with target moving along AC. The x-axis and y-axis are the distance between target and sensor A and $\mathfrak{R}$.

the shape of the distribution of $\mathfrak{R}$ with other σ_ω^2 should be similar to the shape of Figures 5 and 6.

4.2. Evaluation of Average $\mathfrak{R}$. In many localization tasks, it is required to monitor a certain area by a certain number of sensors. Consequently, there arises a question of what the best regular pattern is to deploy these sensors. To solve this problem, it is important to investigate the average localization accuracy of different patterns.

Suppose that, in a given area S, the total number of deployed sensors is N_a; then, the area that a single sensor can cover is $S_0 = S/N_a$. For regular deployment patterns, S_0 satisfies [25]

$$S_0 = \frac{S_p}{N_p} \cdot N_s, \tag{26}$$

where S_p is the area of a regular pattern, N_p stands for the number of sensors that a pattern contains, and N_s denotes the number of patterns that a sensor connects. As we can see in Figure 10, $N_p = 3$, $N_s = 6$ for triangle, $N_p = 4$, $N_s = 4$ for square, and $N_p = 6$, $N_s = 3$ for hexagon.

Let their side lengths be a_3, a_4, and a_6, respectively. Then, we have

$$S_{p3} = \frac{\sqrt{3}}{4} a_3^2, \qquad S_{p4} = a_4^2, \qquad S_{p6} = \frac{3\sqrt{3}}{2} a_6^2, \tag{27}$$

where S_{p3}, S_{p4}, and S_{p6} denote the area of triangle, square, and hexagon, respectively. Consequently, the side length of each regular pattern can be derived as follows:

$$a_3 = \sqrt{\frac{2\sqrt{3}}{3} S_0}, \qquad a_4 = \sqrt{S_0}, \qquad a_6 = \sqrt{\frac{4\sqrt{3}}{9} S_0}. \tag{28}$$

Let $\overline{\mathfrak{R}}$ denote the average $\mathfrak{R}$ inside a certain regular pattern. Figure 11 illustrates the profiles of $\overline{\mathfrak{R}}$ of three regular patterns under different situations, where $\sigma_v^2 = 1$ and the x-axis is S_0 and y-axis is $\overline{\mathfrak{R}}$. The left-top subfigure shows the situation with only additive noise. It is clear that $\overline{\mathfrak{R}}$ of each pattern remains constant despite the increase of S_0, because $\mathfrak{R}$ depends only on the angular diversity other than the target-sensor distance. On the other hand, other subfigures confirm that $\overline{\mathfrak{R}}$ increases with the increase of S_0 under

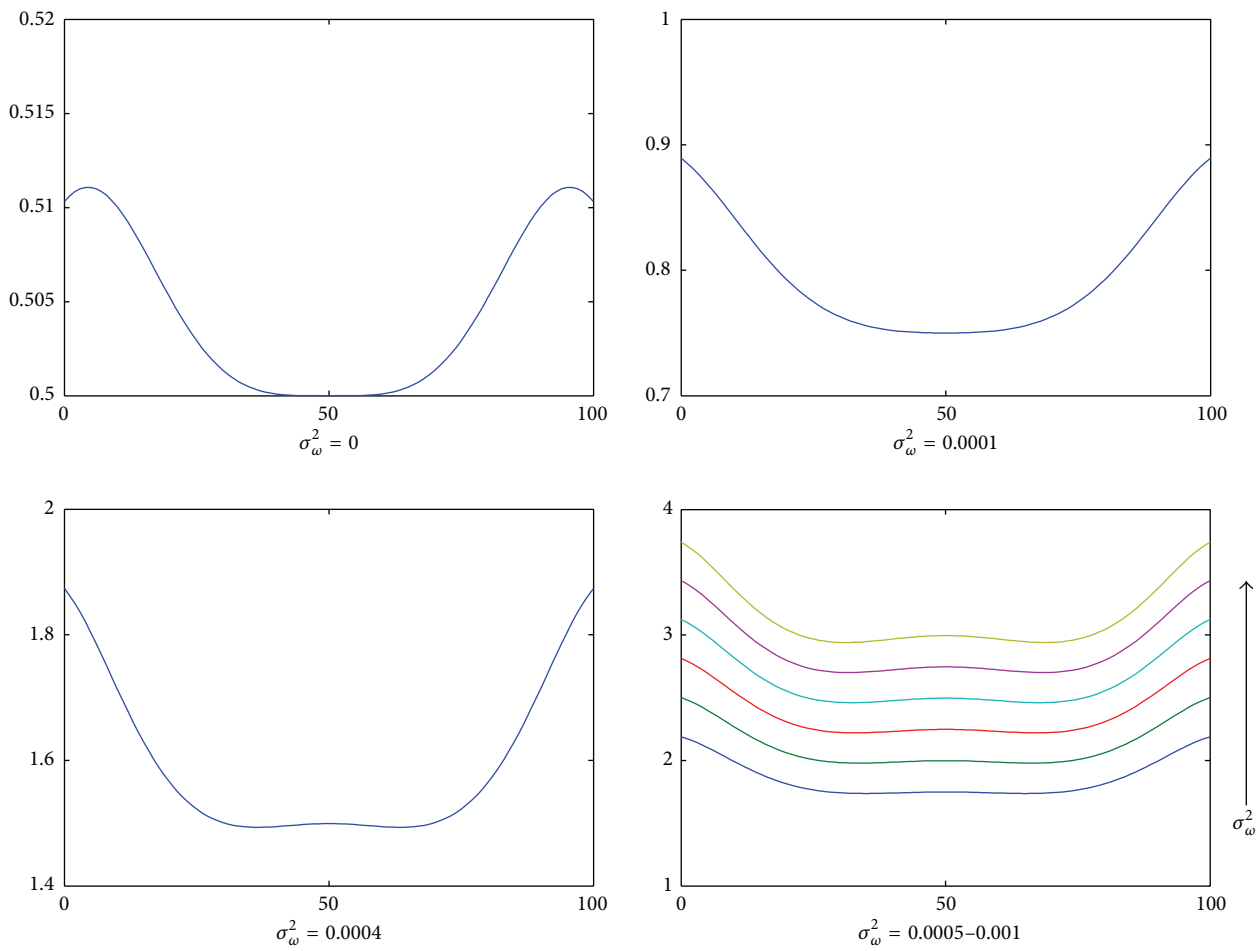

Figure 9: The profiles of $\mathfrak{R}$ under the effect of multiplicative noise with target moving along MN. The x-axis and y-axis are the distance between target and M and $\mathfrak{R}$.

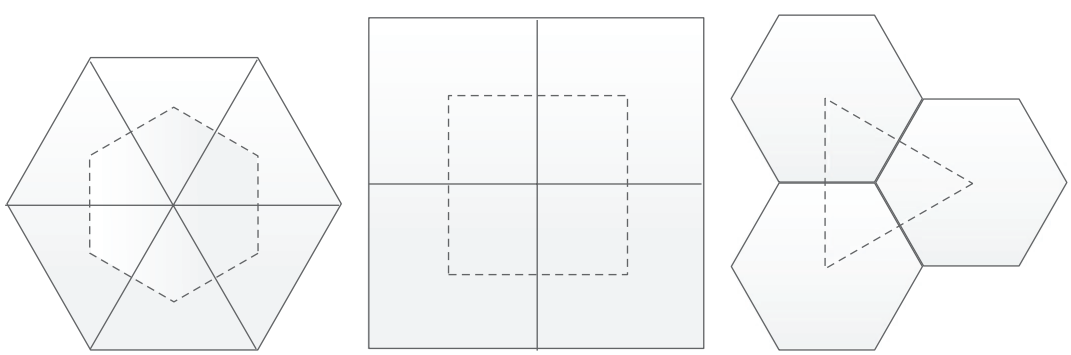

(a) Triangle (b) Square (c) Hexagon

Figure 10: The extension of three kinds of regular deployment patterns.

both additive and multiplicative noises, which is consistent with our common sense. Figure 11 also indicates that the hexagon and the triangle always yield the lowest and highest $\overline{\mathfrak{R}}$, respectively, under all situations. That is, deploying the sensors in a hexagon pattern will lead to the best localization accuracy.

However, though the hexagon pattern obtains the lowest $\overline{\mathfrak{R}}$, it does not mean that the hexagon pattern is the best way to deploy sensors in practice. It is notable that, for the three deployment patterns, the numbers of active sensors are different, that is, $N_{p3} = 3$, $N_{p4} = 4$, $N_{p6} = 6$, which leads to different cost, including energy, communication, and

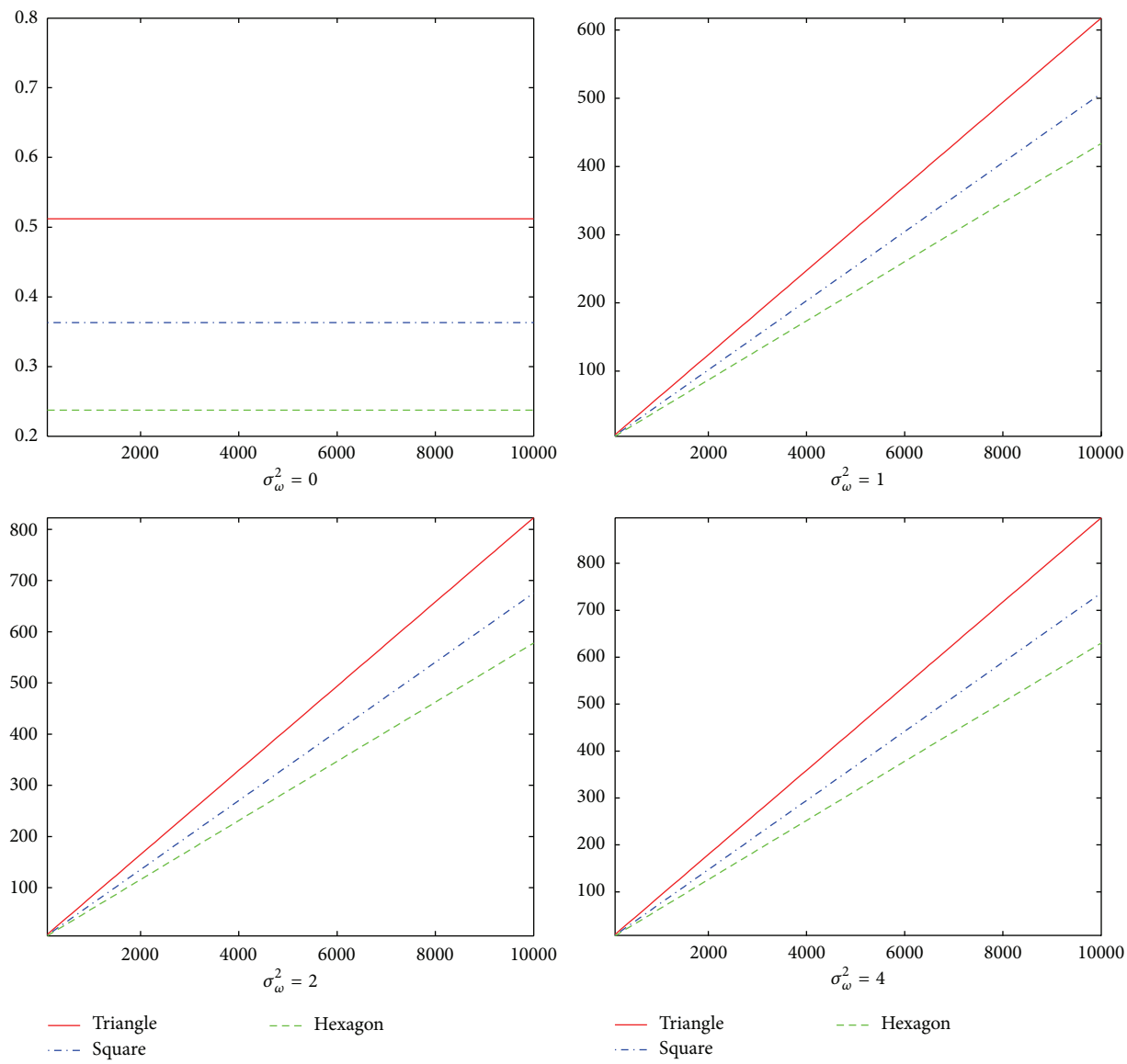

FIGURE 11: The profiles of $\overline{\mathfrak{R}}$ with different σ_ω^2. The x-axis and y-axis are S_0 and $\overline{\mathfrak{R}}$.

computation. Therefore, a new index is desired to represent the normalized average localization accuracy that a single active sensor can contribute. As the lower $\overline{\mathfrak{R}}$ corresponds to the better accuracy, this index can be given as

$$\mathfrak{I} = \overline{\mathfrak{R}} \cdot N_p. \tag{29}$$

The comparison of $\mathfrak{I}$ of these regular patterns is illustrated in Figure 12. From the left-top subfigure with only additive noise, the hexagon pattern has the smallest $\mathfrak{I}$; that is, deploying the sensors in hexagon will yield the best normalized average accuracy. However, if both additive and multiplicative noises are considered and the variance of multiplicative noise is comparable with that of additive noise, the results are completely different. That is, the triangle pattern owns the best normalized average localization accuracy, while the hexagon pattern yields the worst.

Remark 7. In practice, the localization accuracy and other factors may be combined together for optimal sensor deployment. Different weights can be utilized to reflect the preference of designer under different situations. However, the same methodology can be applied to obtain the tradeoff between localization accuracy and other concerns.

5. Experimental Verification

A lab-scale experiment is set up to illustrate, first, the existence of additive noise and multiplicative noise and, then, the profiles of $\mathfrak{R}$ of a moving target. The ultrasonic range-only sensors are used in this experiment, which consists of three modules: core microprocessor Atmegal128L, wireless communication module CC2420, and ultrasonic sensor module URM37 V3.2.

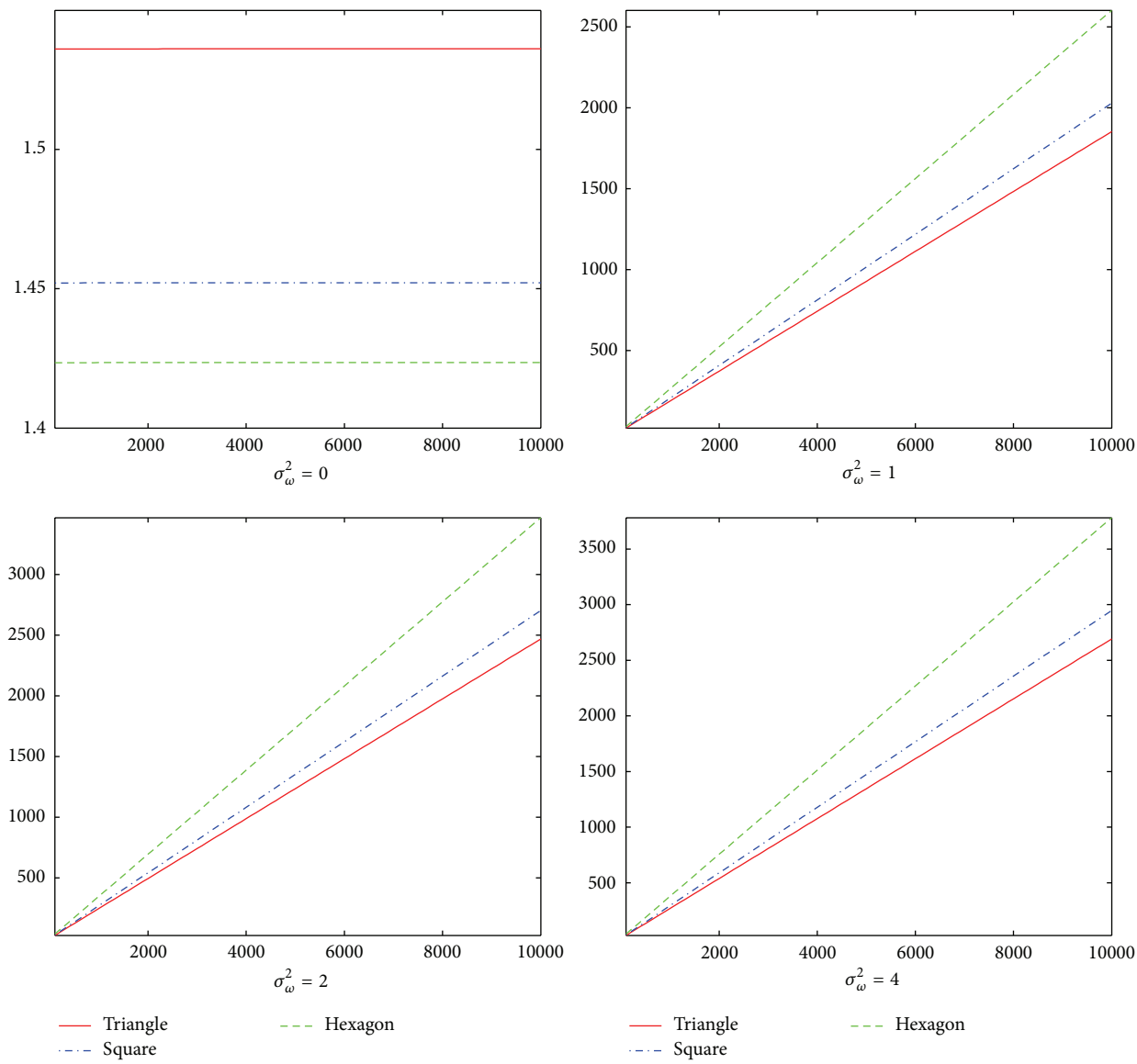

Figure 12: The profiles of $\mathfrak{I}$ with different σ_ω^2. The x-axis and y-axis are S_0 and $\mathfrak{I}$.

In order to show the existence of additive and multiplicative noises and compute the corresponding means and variances, a 0.05 m × 0.05 m × 0.1 m rectangular target is placed in the front of an ultrasonic range-only sensor from 0.1 m to 2 m for every 0.1 m. At each point, 600 distance readings are recorded. Based on (3) and (4) and following the least square fitting procedure detailed in [2], we can readily obtain for additive noise $\mu_\upsilon = -0.00072489$, $\sigma_\upsilon^2 = 0.04401$ and for multiplicative noise $\mu_\omega = 0.01597$, $\sigma_\omega^2 = 0.07251$. It is clear that the variance of multiplicative noise is even larger than that of additive noise. However, the sensor is not unbiased. Figure 13 shows 300 distance readings when the true target-sensor distance is 1.2 m. We can see that the existence of multiplicative noise and additive noise will bring biases to the distance measurements.

In order to show the profiles of $\mathfrak{R}$ of a moving target, we set up a 1.2 m × 1.2 m square deployment with 4 ultrasonic range-only sensors for the ease of manipulating, as shown in Figure 3(b). The experimental testbed is shown in Figure 14. Now, we will move a round target with diameter of 0.1 m along diagonal line AC and midline MN, respectively, for every 0.1 m. At each point, 250 sets of distance readings will be recorded. For each set of readings, it consists of the distance measurements of 4 sensors, which can be used to readily estimate the target location. Consequently, the empirical variance matrix of localization error can be obtained for each point, as well as its determinant that is plotted in Figures 15 and 16. Meanwhile, $\mathfrak{R}$ also can be computed based on (16) for each point and plotted in Figures 15 and 16, with $\sigma_\upsilon^2 = 0.04401$ and $\sigma_\omega^2 = 0.07251$. It is clear that the experimental profiles are close to the theoretical ones. It is also noticed that the determinant of variance matrix is constantly larger than $\mathfrak{R}$ for all points. Because $\mathfrak{R}$ is derived from CRLB that is the lower bound of any unbiased estimator, $\mathfrak{R}$ only reflects the lower

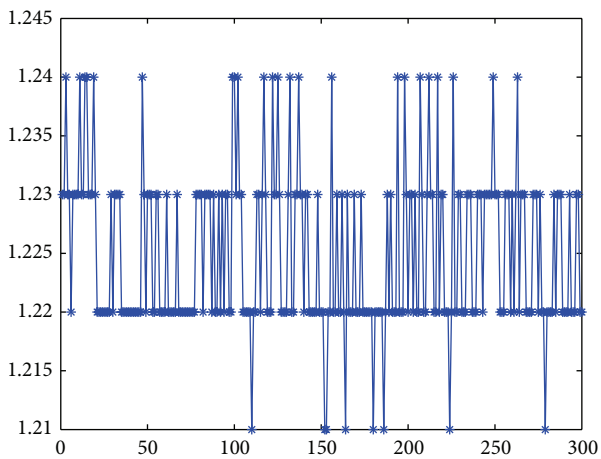

Figure 13: Distance measurements, true target-sensor distance is 1.2 m.

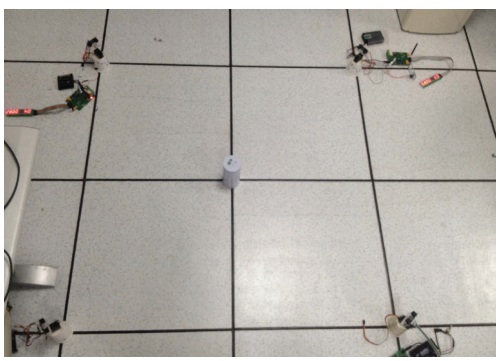

Figure 14: Experimental testbed consisting of four ultrasonic range-only sensors and a round target with radius as 0.05 m.

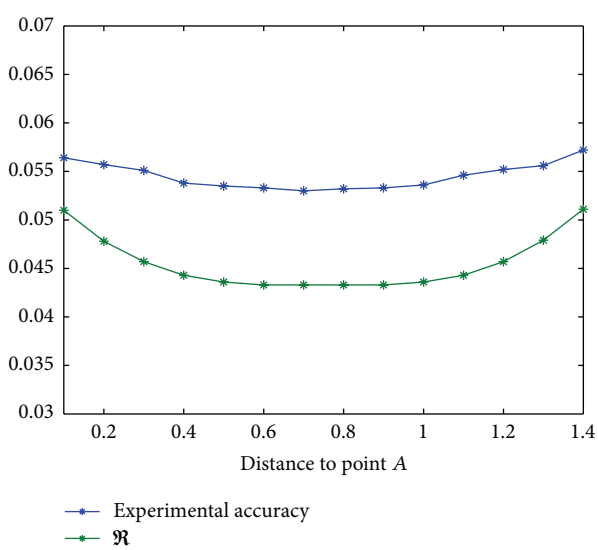

Figure 15: The profiles of experimental localization accuracy and $\mathfrak{R}$ for a target moving along diagonal line AC.

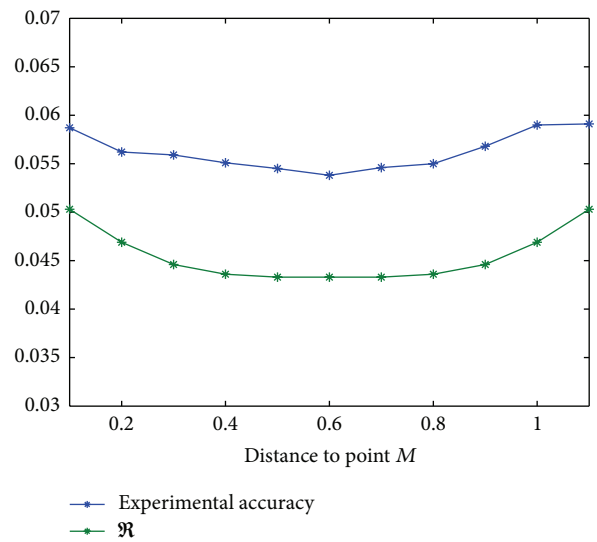

Figure 16: The profiles of experimental localization accuracy and $\mathfrak{R}$ for a target moving along midline MN.

bound of unbiased localization. In addition, the ultrasonic range-only sensor itself is biased, which may also increase the variance.

6. Conclusion

This paper studies the issue of localization accuracy for range-only sensors with both additive and multiplicative noises. The CRLB of the localization system and a novel metric $\mathfrak{R}$ of CRLB are derived. Then, three analytical properties of $\mathfrak{R}$ are derived, which are helpful for us to understand the underlying relationships between target-sensor distance and localization accuracy, as well as between noise and localization accuracy. In particular, two unexpected results about the relationships are found.

Then, the localization accuracy for three regular deployment patterns, including triangle, square, and hexagon, is evaluated numerically in terms of $\mathfrak{R}$. It shows that the existence of multiplicative noise will significantly change the geometric distribution of localization accuracy. The average localization accuracy is also examined, and the results indicate that the hexagon always has the best average accuracy, no matter whether multiplicative noise exists or not. However, if the average accuracy is normalized by the number of active sensors, the results suggest that the triangle would be the best regular pattern to deploy the sensors.

At last, lab-scale experiment is carried out to illustrate the existence of additive and multiplicative noises. It is also shown that the experimental localization accuracy is close to $\mathfrak{R}$, which nicely verifies the previous theoretical analysis.

Conflict of Interests

The authors declare that there is no conflict of interests regarding the publication of this paper.

Acknowledgments

This work was supported by 973 Program under Grant 2013CB329503 and NSFC under Grant 61371159.

References

[1] B. S. Yaakov, X. Li, and T. Kirubarajan, *Estimation with Application to Tracking and Navigation*, Wiley, New York, NY, USA, 2001.

[2] X. Wang, M. Fu, and H. Zhang, "Target tracking in wireless sensor networks based on the combination of KF and MLE using distance measurements," *IEEE Transactions on Mobile Computing*, vol. 11, no. 4, pp. 567–576, 2012.

[3] Y. Cheng, X. Wang, T. Caelli, X. Li, and B. Moran, "Optimal nonlinear estimation for localization of wireless sensor networks," *IEEE Transactions on Signal Processing*, vol. 59, no. 12, pp. 5674–5685, 2011.

[4] L. Dong, "Cooperative localization and tracking of mobile ad hoc networks," *IEEE Transactions on Signal Processing*, vol. 60, no. 7, pp. 3907–3913, 2012.

[5] N. Kantas, S. S. Singh, and A. Doucet, "Distributed maximum likelihood for simultaneous self-localization and tracking in sensor networks," *IEEE Transactions on Signal Processing*, vol. 60, no. 10, pp. 5038–5047, 2012.

[6] G. Gaderer, P. Loschmidt, A. Nagy, R. Exel, and T. Sauter, "Localisation in wireless sensor networks," *IEEE Sensors*, vol. 22, no. 4, pp. 54–69, 2005.

[7] S. Martínez and F. Bullo, "Optimal sensor placement and motion coordination for target tracking," *Automatica*, vol. 42, no. 4, pp. 661–668, 2006.

[8] F. Zhao, J. Shin, and J. Reich, "Information-driven dynamic sensor collaboration," *IEEE Signal Processing Magazine*, vol. 19, no. 2, pp. 61–72, 2002.

[9] H. Wang, K. Yao, and D. Estrin, "Information-theoretic approaches for sensor selection and placement in sensor networks for target localization and tracking," *Journal of Communications and Networks*, vol. 7, no. 4, pp. 438–449, 2005.

[10] A. N. Bishop, B. Fidan, B. D. O. Anderson, K. Doğançay, and P. N. Pathirana, "Optimality analysis of sensor-target localization geometries," *Automatica*, vol. 46, no. 3, pp. 479–492, 2010.

[11] L. M. Kaplan, "Global node selection for localization in a distributed sensor network," *IEEE Transactions on Aerospace and Electronic Systems*, vol. 42, no. 1, pp. 113–135, 2006.

[12] B. Ristic and M. S. Arulampalam, "Tracking a manoeuvring target using angle-only measurements: algorithms and performance," *Signal Processing*, vol. 83, no. 6, pp. 1223–1238, 2003.

[13] M. Steven Kay, *Fundamentals of Statistical Signal Processing: Estimation Theory*, vol. 1, 1993.

[14] Z. Yang, C. W. Chan, and Y. Wang, "A high-accuracy detection and estimation method of intermodulated sinusoids," *IEEE Transactions on Circuits and Systems I*, vol. 58, no. 10, pp. 2477–2484, 2011.

[15] Z. Yang and C. W. Chan, "On estimation of intermodulated frequencies for sinusoidal signals with unknown fundamental frequencies," *IEEE Transactions on Signal Processing*, vol. 57, no. 8, pp. 3279–3283, 2009.

[16] Z. Yang and C. W. Chan, "Simultaneous estimation of the input and output frequencies of nonlinear systems," *Automatica*, vol. 44, no. 7, pp. 1822–1830, 2008.

[17] H. Godrich, A. P. Petropulu, and H. V. Poor, "Sensor selection in distributed multiple-radar architectures for localization: a knapsack problem formulation," *IEEE Transactions on Signal Processing*, vol. 60, no. 1, pp. 247–260, 2012.

[18] T. Zhao and A. Nehorai, "Information-driven distributed maximum likelihood estimation based on Gauss-Newton method in wireless sensor networks," *IEEE Transactions on Signal Processing*, vol. 55, no. 9, pp. 4669–4682, 2007.

[19] D. Uciński, "Optimal sensor location for parameter estimation of distributed processes," *International Journal of Control*, vol. 73, no. 13, pp. 1235–1248, 2000.

[20] K. Doğançay and H. Hmam, "Optimal angular sensor separation for AOA localization," *Signal Processing*, vol. 88, no. 5, pp. 1248–1260, 2008.

[21] J. N. Ash and R. L. Moses, "On the relative and absolute positioning errors in self-localization systems," *IEEE Transactions on Signal Processing*, vol. 56, no. 11, pp. 5668–5679, 2008.

[22] M. Zoghi and M. H. Kahaei, "Adaptive sensor selection in wireless sensor networks for target tracking," *IET Signal Processing*, vol. 4, no. 5, pp. 530–536, 2010.

[23] J. M. Francos, "Cramér-Rao bound on the estimation accuracy of complex-valued homogeneous Gaussian random fields," *IEEE Transactions on Signal Processing*, vol. 50, no. 3, pp. 710–724, 2002.

[24] Z. Ben-Haim and Y. C. Eldar, "The Cramér-Rao bound for estimating a sparse parameter vector," *IEEE Transactions on Signal Processing*, vol. 58, no. 6, pp. 3384–3389, 2010.

[25] X. Bai, S. Kumar, D. Xuan, Z. Yun, and T. H. Lai, "Deploying wireless sensors to achieve both coverage and connectivity," in *Proceedings of the 7th ACM International Symposium on Mobile Ad Hoc Networking and Computing (MOBIHOC '06)*, pp. 131–142, May 2006.

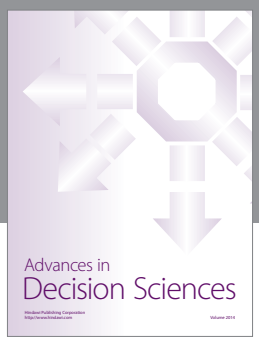

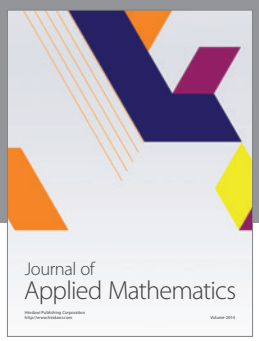

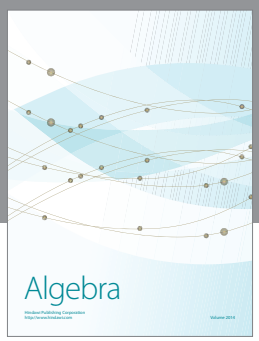

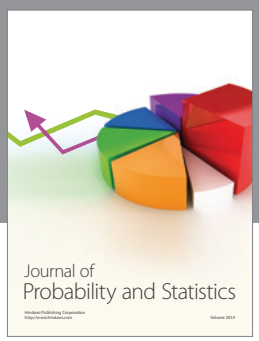

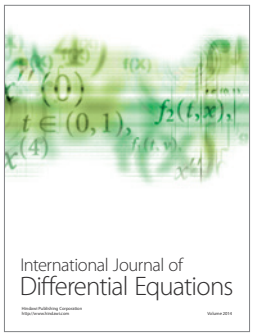

Hindawi

Submit your manuscripts at
http://www.hindawi.com